Supplementary Information:

Phosphorous containing inverse vulcanised sulfur polymers as Li-sulfur positive electrodes

Haoran Wang[†a,b], Pan Yang[†a,b], Alex R. Neale[a,b], Liam J. Dodd[a], Peiyao Yan[a], Bowen Zhang[a], Laurence J. Hardwick[a,b,*], and Tom Hasell[a,b,*]

[a] Department of Chemistry, Oxford Street, University of Liverpool, Liverpool L69 7ZD, UK.

[b] Stephenson Institute for Renewable Energy, Department of Chemistry, Peach Street, University of Liverpool, Liverpool L69 7ZF, UK.

Materials characterisation

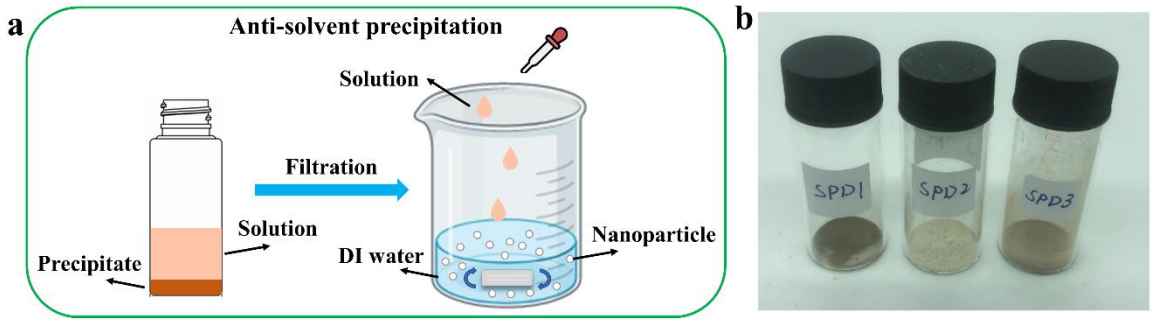

Figure. S1. (a) The scheme of anti-solvent precipitation to prepare SPD nanoparticles. (b) Photograph of SPD1, SPD2 and SPD3 specimens in 14 ml glass vials.

Synthesis of diphenyl (4-vinylphenyl) phosphine sulfide (ref).[1]

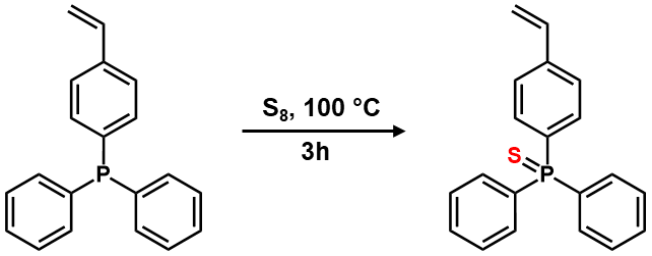

Toluene (30 mL) was added to a round-bottom flask charged with S_8 (0.11 g, 3.5 mmol, 1.00 equiv) and 4-(diphenylphosphino) styrene (D4VPP, 1.0 g, 3.5 mmol, 1.00 equiv). The clear solution was heated at 110 °C for 3 h. Afterward, the solution was concentrated to 15 mL, giving a small amount of colorless precipitate, which was redissolved upon heating. A layer of pentane (15 mL) was carefully added on top of the solution, and the mixture was then stored in a -20 °C freezer overnight to afford the product as colorless needle-like crystals (0.74 g, 67% yield). The ^{1}H, ^{13}C and ^{31}P NMR spectra of D4VPP-S in $CDCl_3$ were exhibited in Figure S2-S4. CI-MS: Calculated $C_{20}H_{17}SP$ $[M+H]^+$ 321.0862, found: 321.0870.

Synthesis of diphenyl (4-vinylphenyl) phosphine oxide.[2]

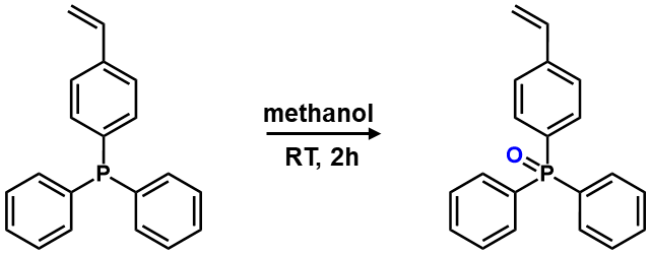

4-(diphenylphosphino) styrene (D4VPP, 17.4 mmol, 5.00 g) was added to a round-bottom flask and dissolved in 1,2-dichloroethane (100 mL). An aqueous solution of saturated potassium peroxymonosulfate (34.8 mmol, 21.4 g) and methanol (20 mL) were then added to the reaction flask, and the mixture was stirred for approximately 2 h. The reaction mixture was poured into a separatory funnel with a large amount of water, and the two layers were separated. The organic phase was collected and concentrated under reduced pressure to afford the white

product D4VPP-O in 92% yield. The ^{1}H, ^{13}C and ^{31}P NMR spectra of D4VPP-O in $CDCl_3$ were exhibited in Figure S5-S7. CI-MS: Calculated $C_{20}H_{17}OP$ $[M+H]^+$ 305.1089, found: 305.1092.

Synthesis of SD4VPP-S and SD4VPP-O polymers

SD4VPP-S and SD4VPP-O were synthesized following the same procedure as SPD. 100 mg sulfur powder (Brenntag) was mixed with 100 mg D4VPP-S/ D4VPP-O in a 5 ml glass vial. The mixture was then heated to 140 ℃ until complete melting of sulfur had occurred. The reaction proceeded with 900 rpm stirring for ca. 12 mins at 180 °C. The resulting viscous sample was cured at 140 °C in an oven for 24 h to obtain a crosslinked polymer. The ^{1}H, ^{13}C and ^{31}P NMR spectra of SD4VPP-S / SD4VPP-O in $CDCl_3$ were exhibited in Figure S8-S13.

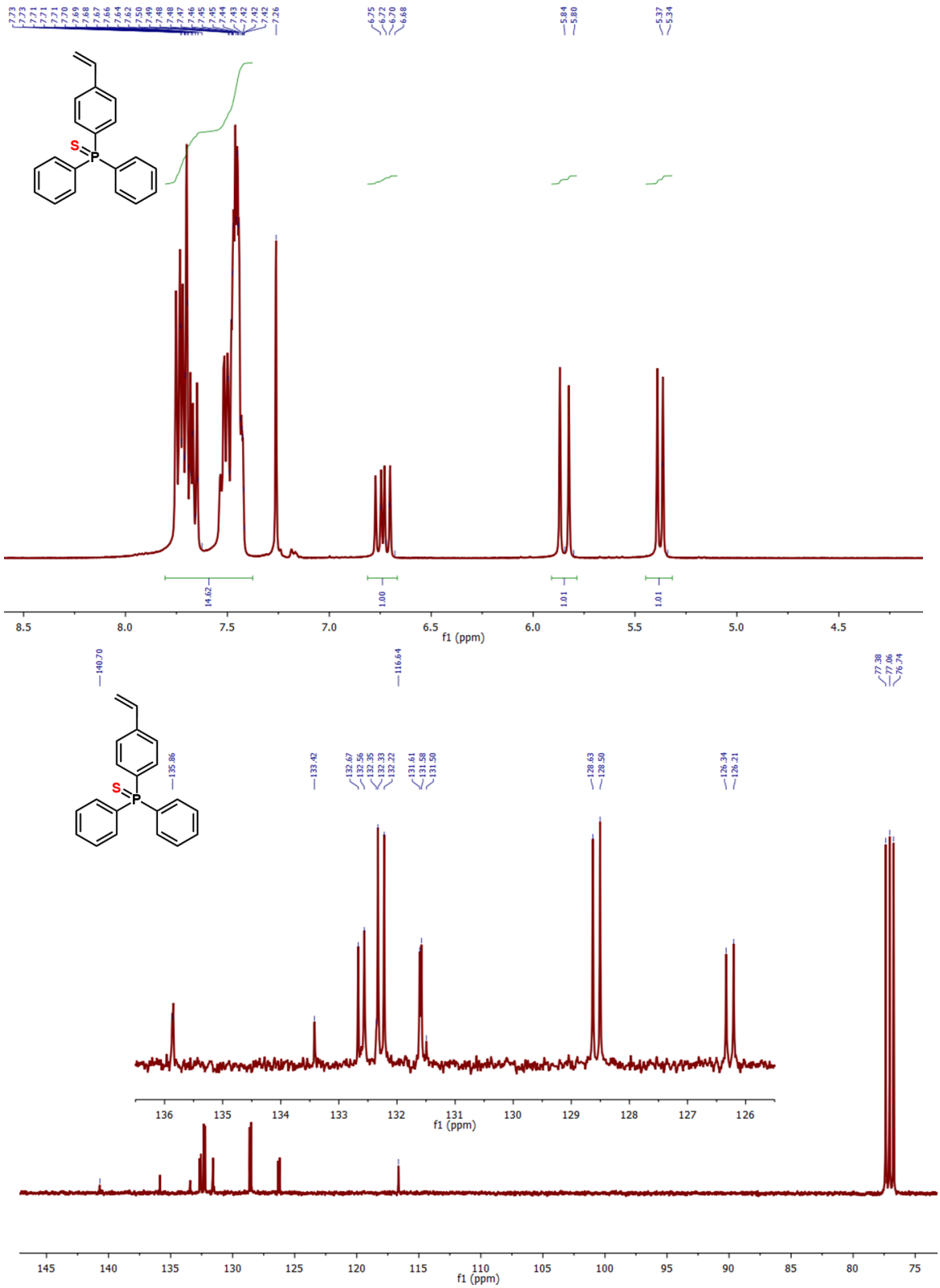

Figure S2. ^{1}H and ^{13}C liquid-state NMR spectra of compound D4VPP-S in $CDCl_3$.

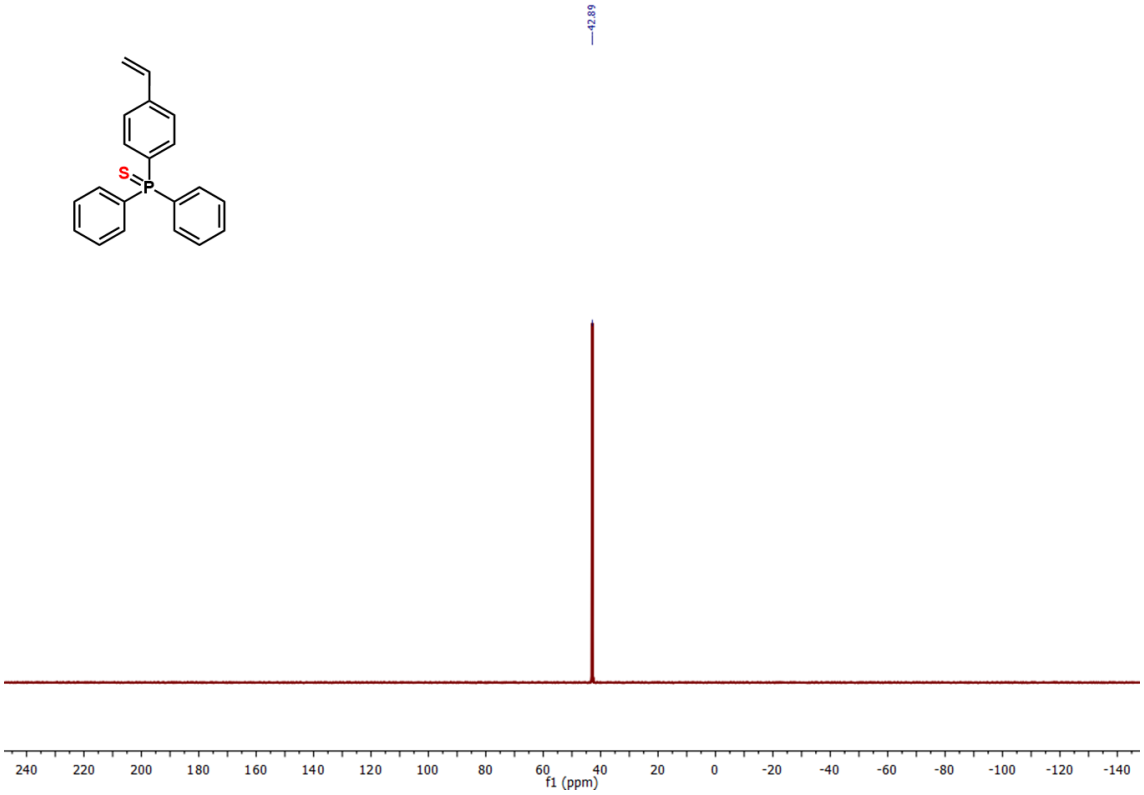

Figure S3. ^{31}P liquid-state NMR spectra of compound D4VPP-S in $CDCl_3$.

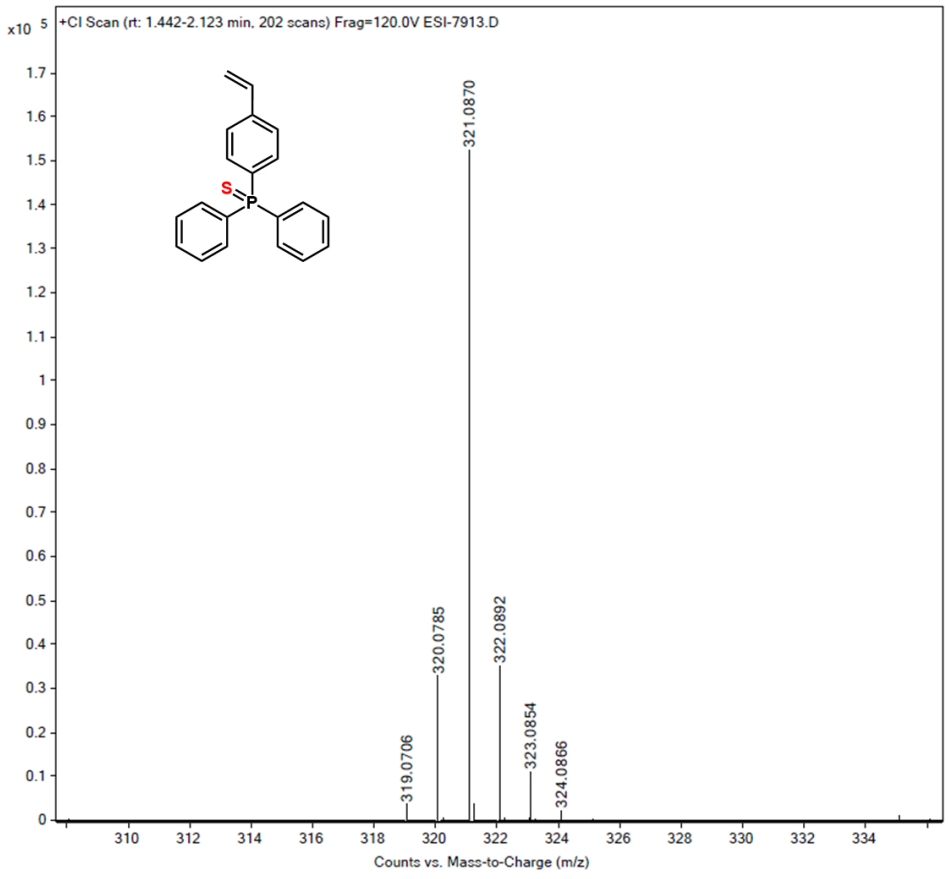

Figure S4. CI-MS of compound D4VPP-S.

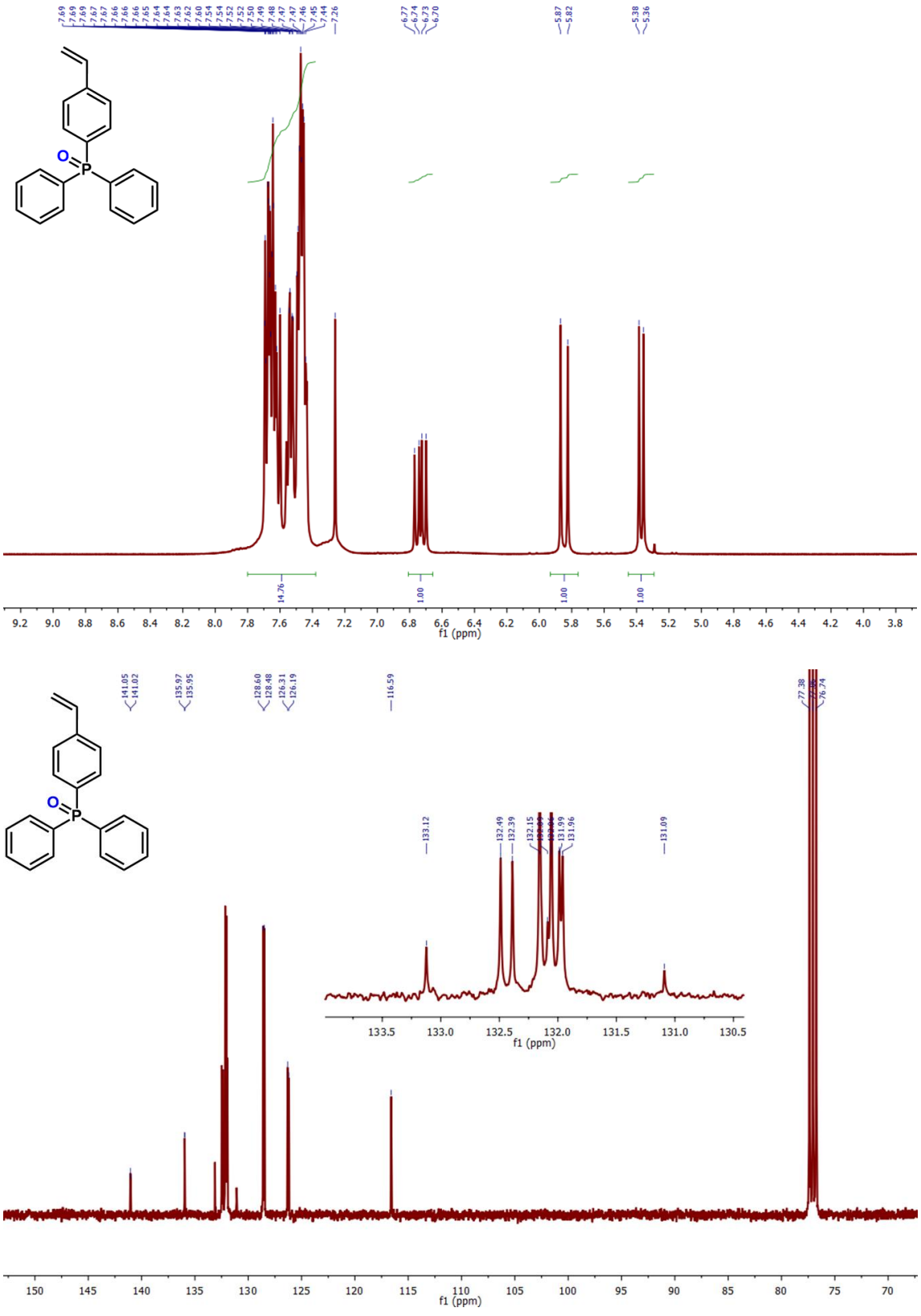

Figure S5. ^{1}H and ^{13}C liquid-state NMR spectra of compound D4VPP-O in $CDCl_3$.

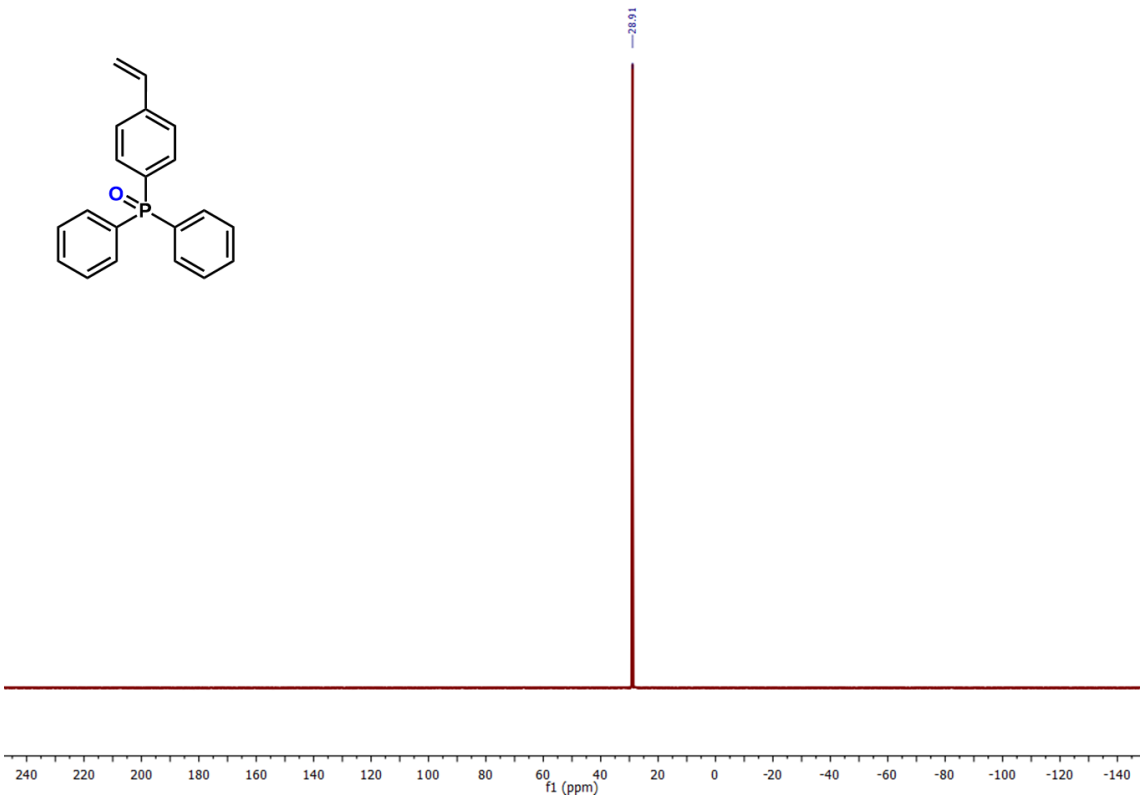

Figure S6. ^{31}P liquid-state NMR spectra of compound D4VPP-O in $CDCl_3$.

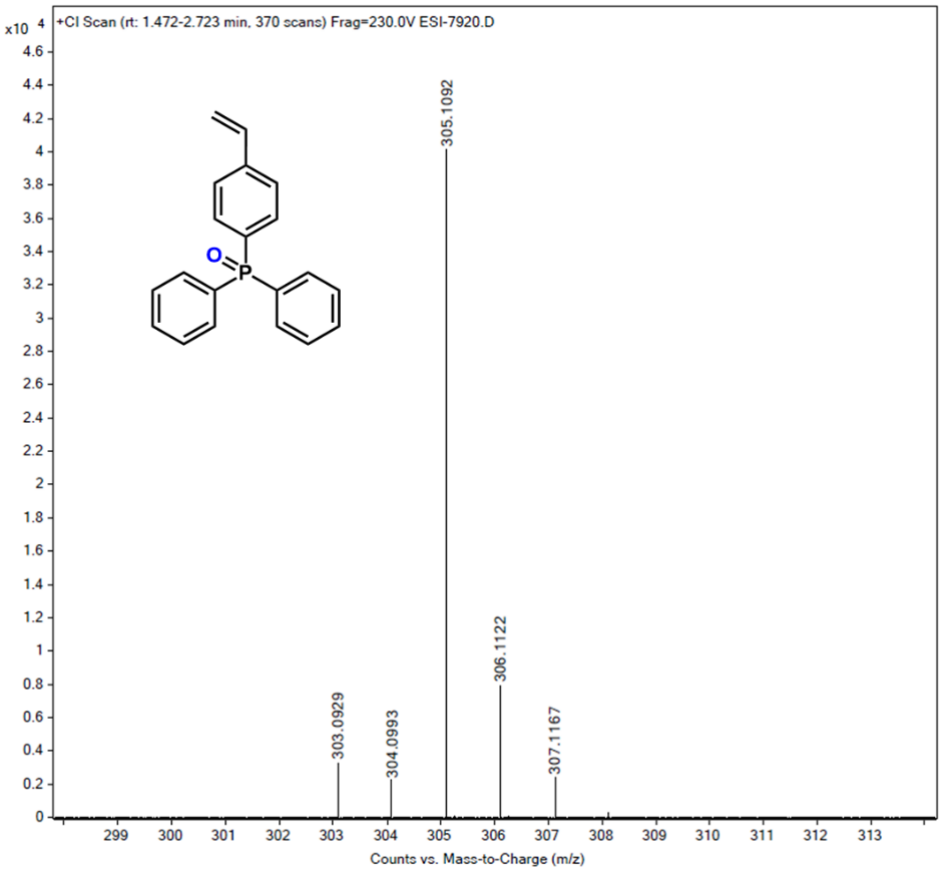

Figure S7. CI-MS of compound D4VPP-O.

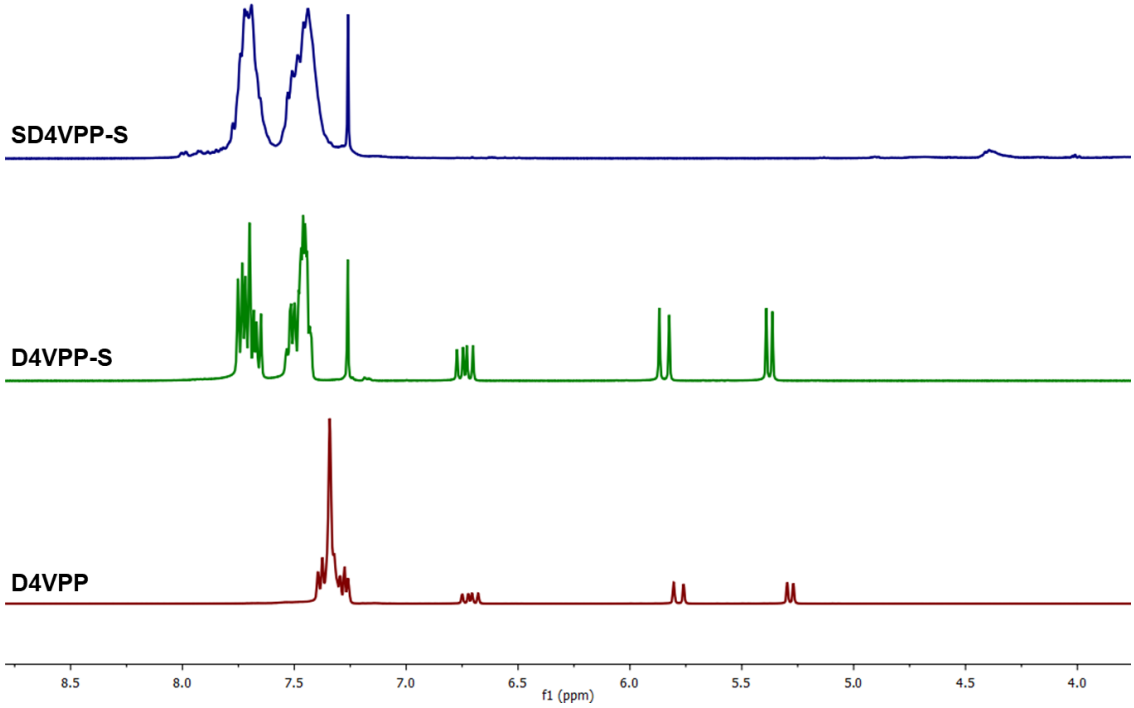

Figure S8. ^{1}H NMR spectra of D4VPP, D4VPP-S, and SD4VPP-S in $CDCl_3$. Broad peaks in SD4VPP-S confirm polymer formation.

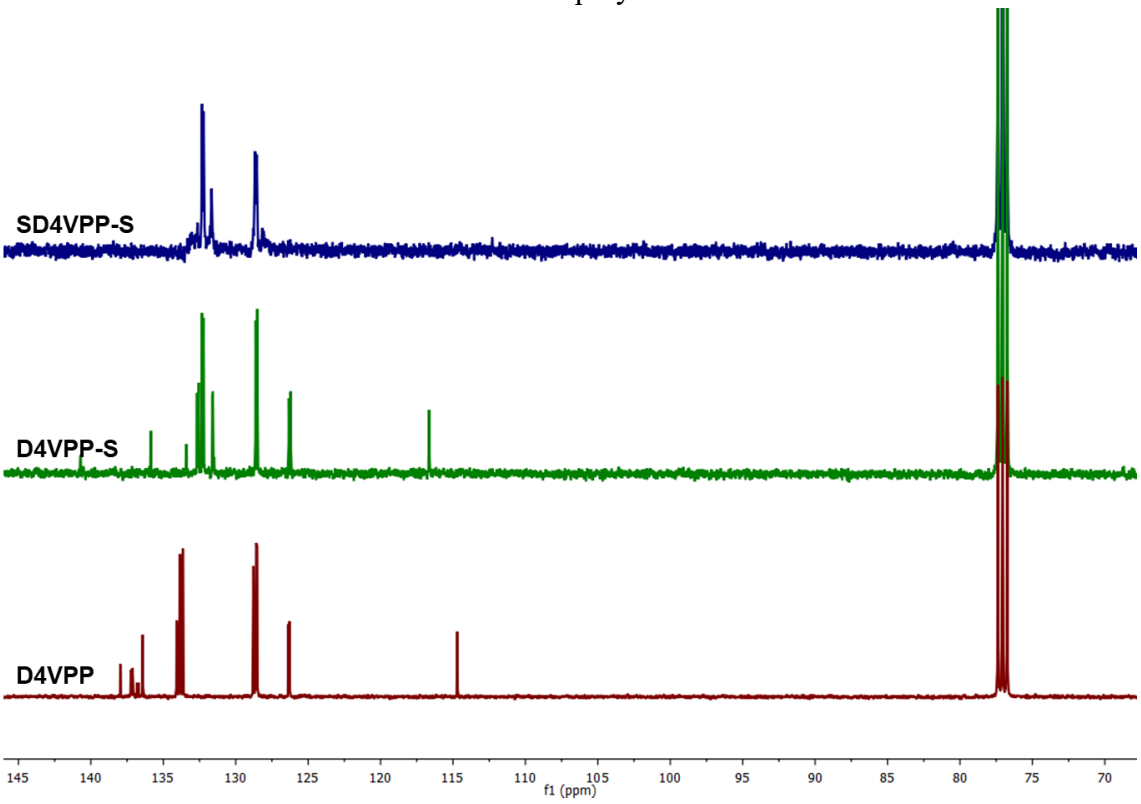

Figure S9. ^{13}C NMR spectra of D4VPP, D4VPP-S, and SD4VPP-S in $CDCl_3$.

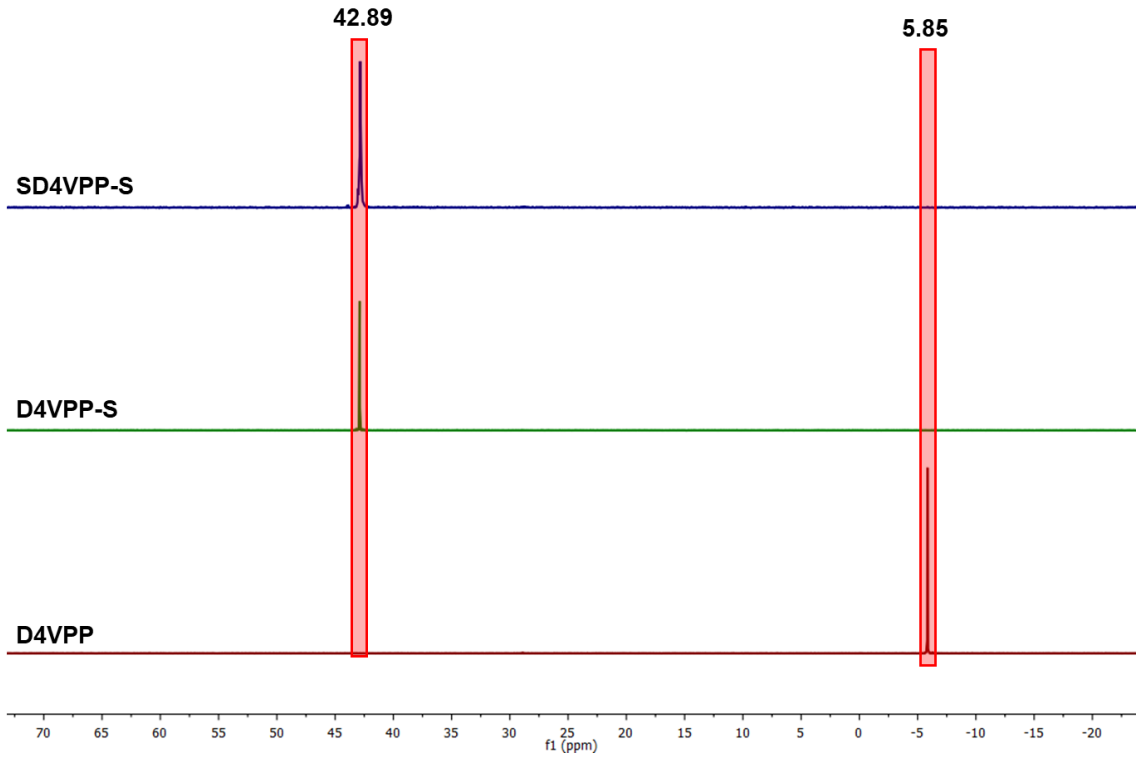

Figure S10. ^{31}P NMR spectra of D4VPP, D4VPP-S, and SD4VPP-S in $CDCl_3$.

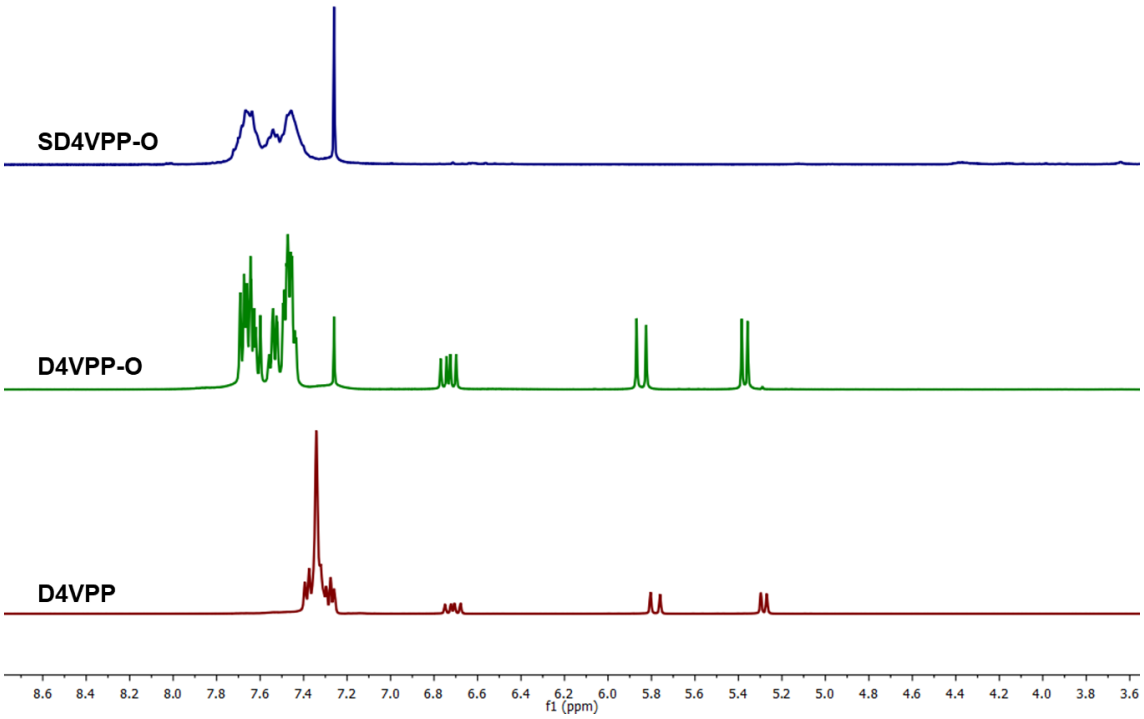

Figure S11. ^{1}H NMR spectra of D4VPP, D4VPP-O, and SD4VPP-O in $CDCl_3$. Broad peaks in SD4VPP-O confirm polymer formation.

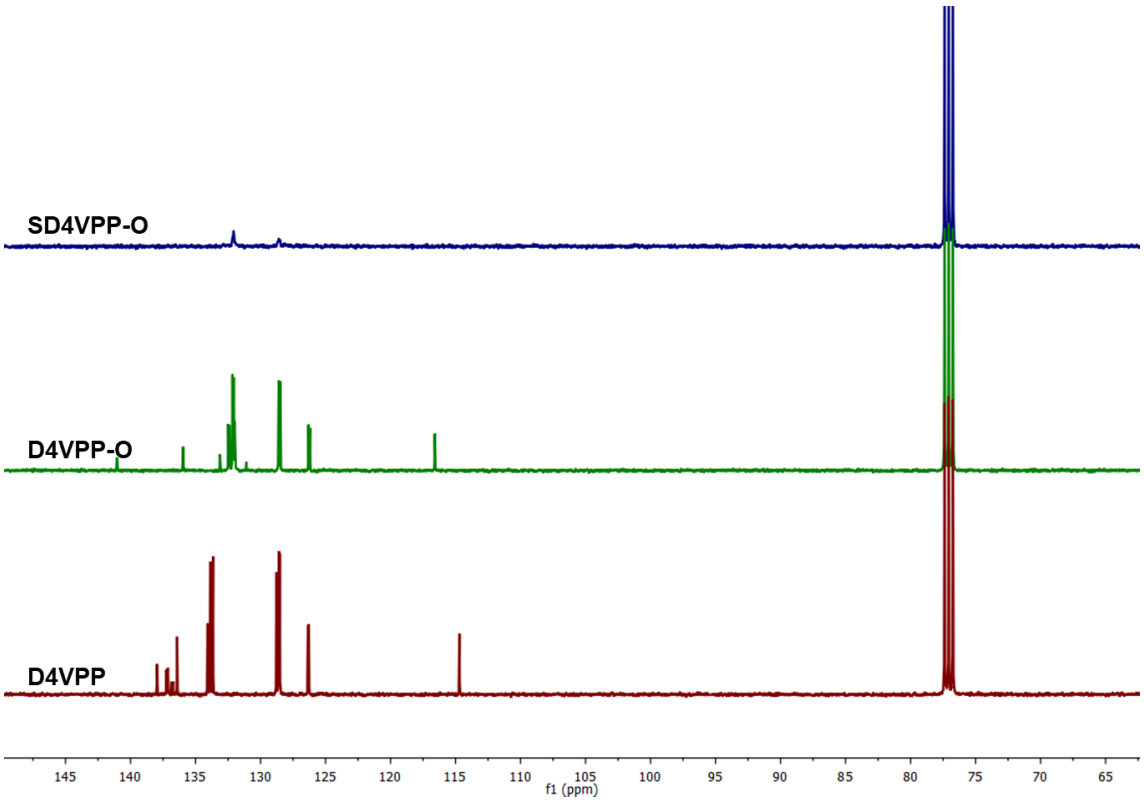

Figure S12. ^{13}C NMR spectra of D4VPP, D4VPP-O, and SD4VPP-O in $CDCl_3$.

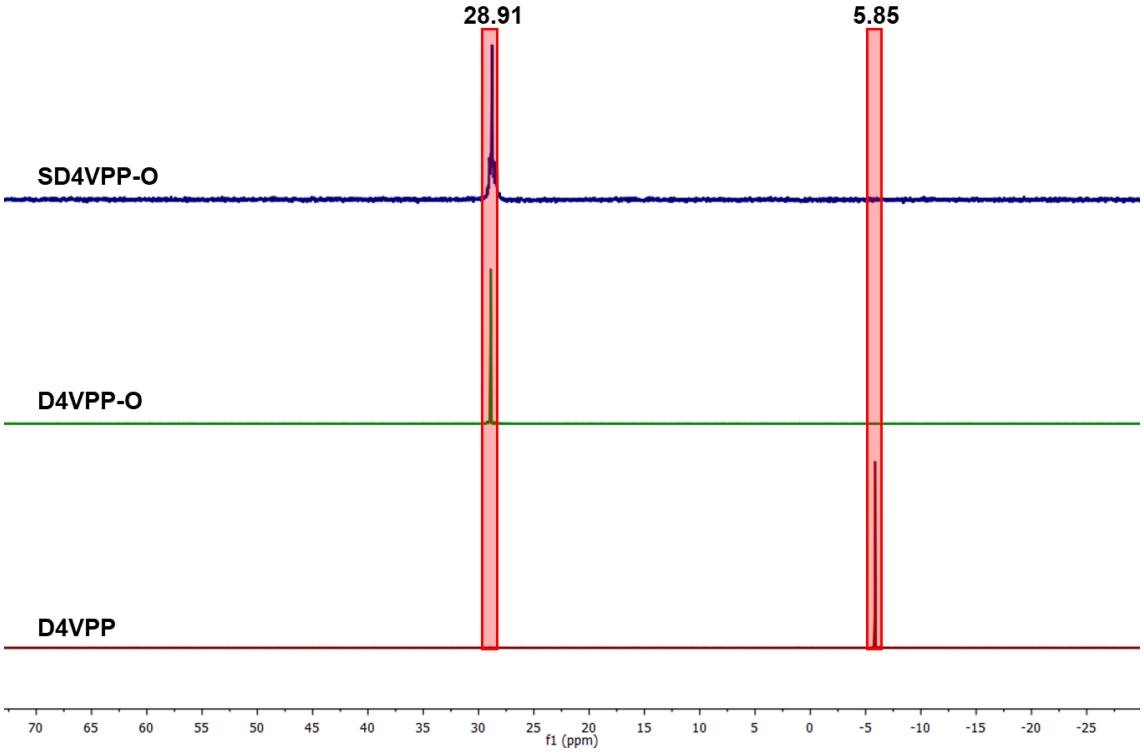

Figure S13. ^{31}P NMR spectra of D4VPP, D4VPP-O, and SD4VPP-O in $CDCl_3$.

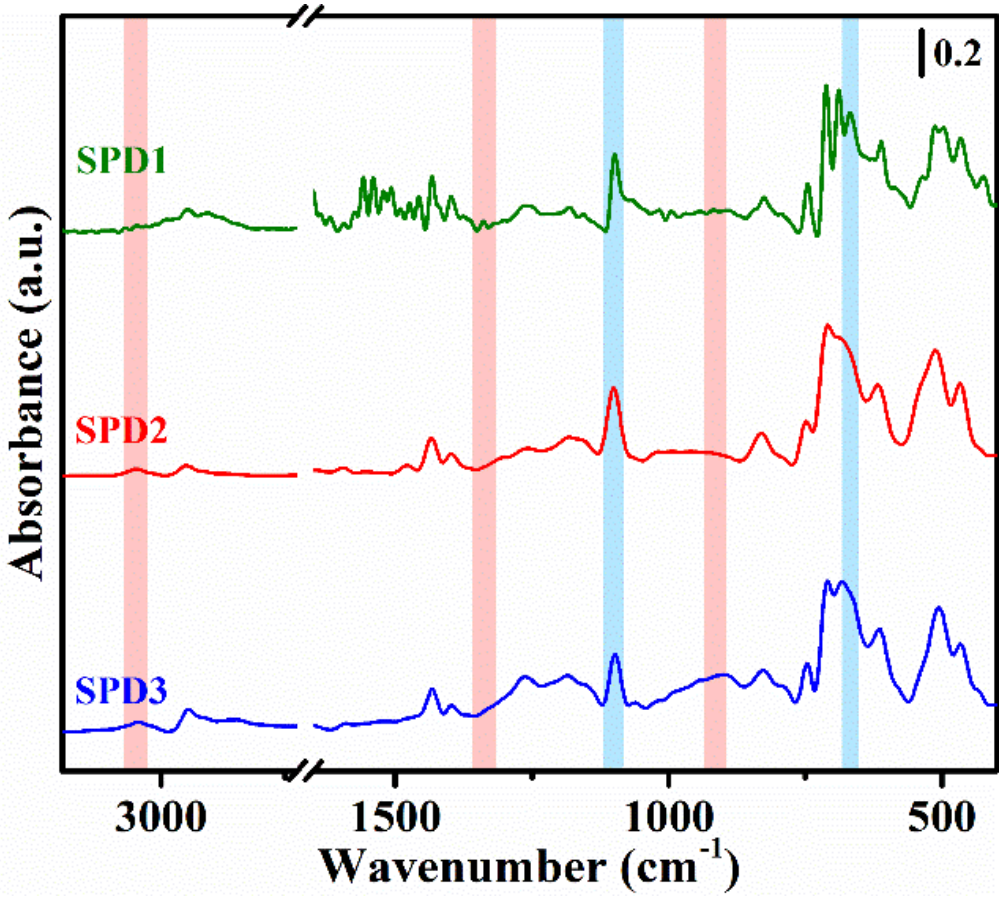

Figure S14. FTIR spectra of SPD1, SPD2 and SPD3.

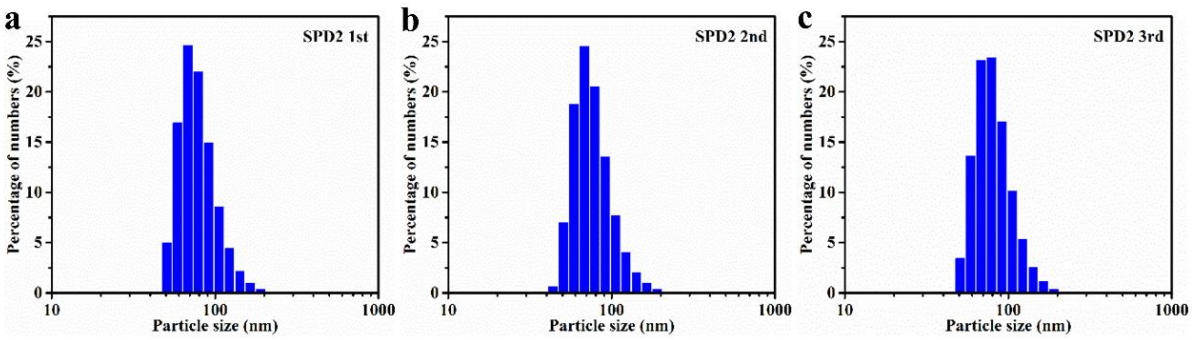

Figure. S15. The obtained size distribution by DLS analysis for three SPD2 samples.

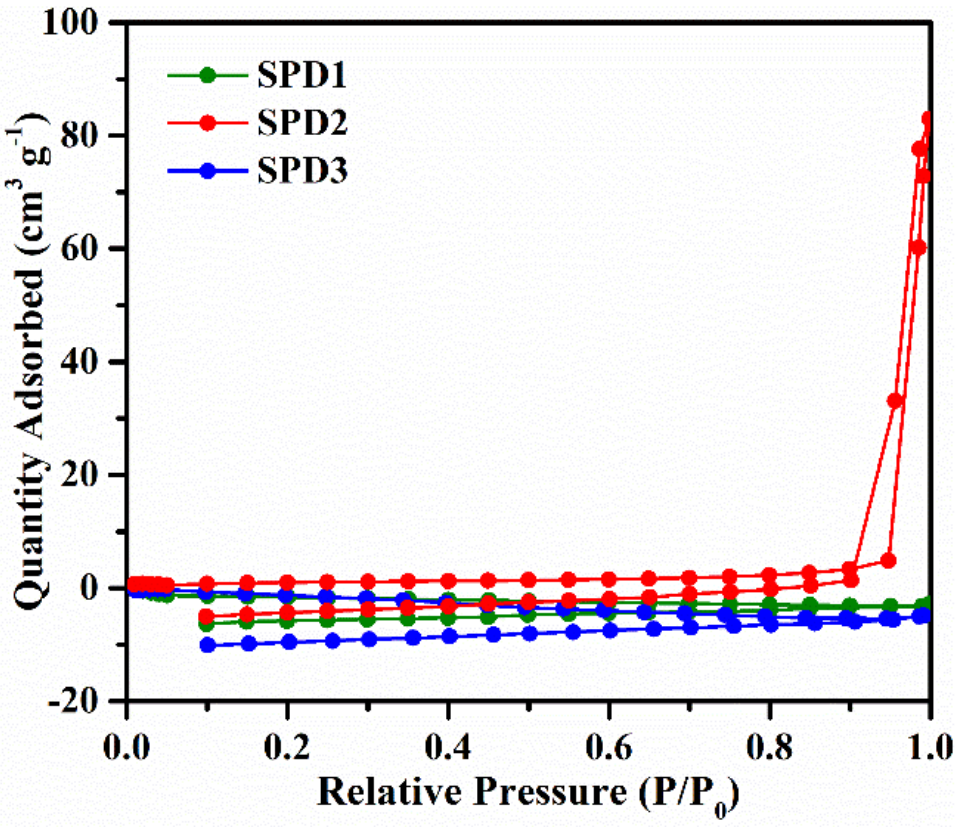

Figure S16. The N_2 adsorption/desorption isotherm of the obtained SPD samples from Brunauer-Emmett-Teller (BET) measurements.

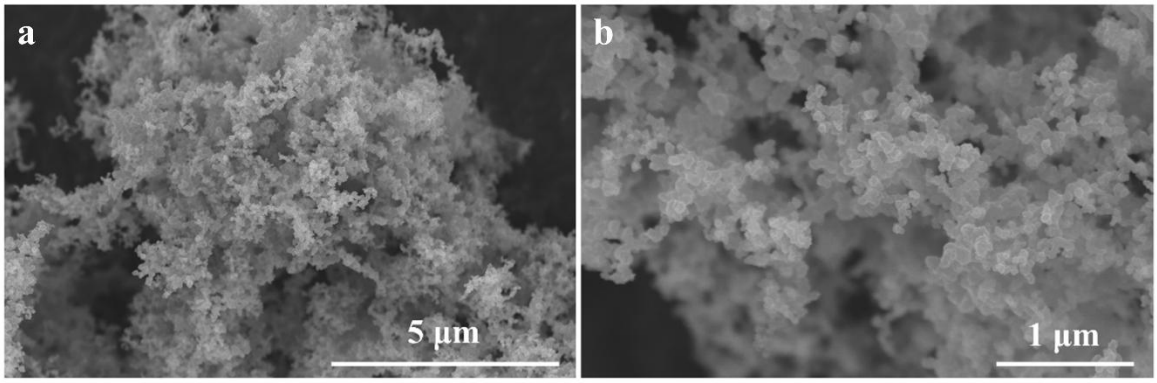

Figure S17. SEM images of acetylene black.

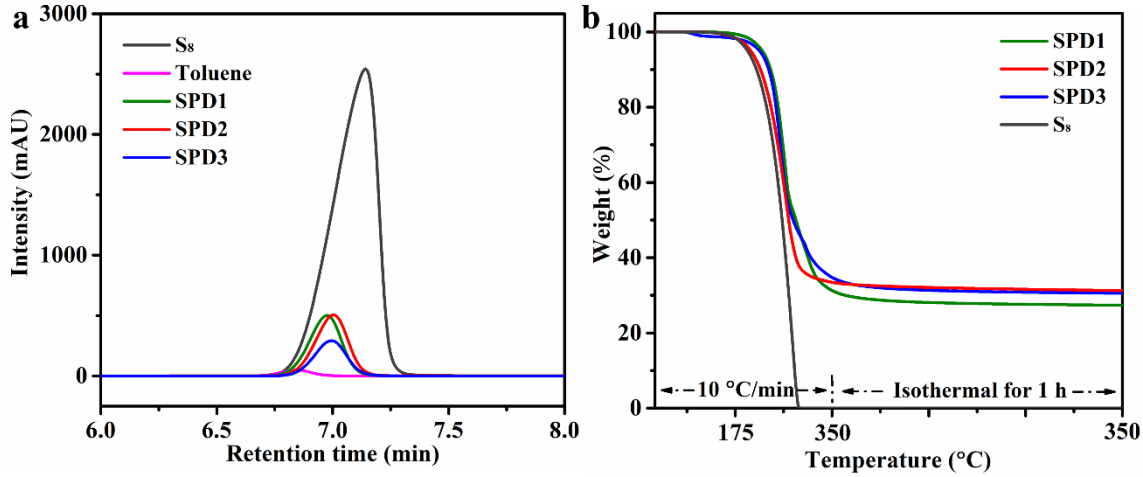

Figure S18. (a) HPLC and (b) TGA results of the SPD samples.

Electrochemical performance

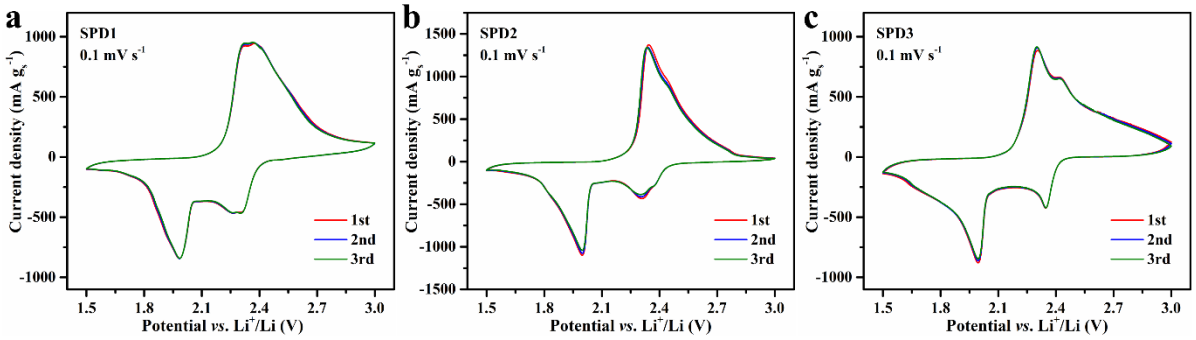

Figure S19. CV curves with scan rate of 0.1 mV s^{-1} for 3 cycles of the cells based on (a) SPD1, (b) SPD2 and (c) SPD3.

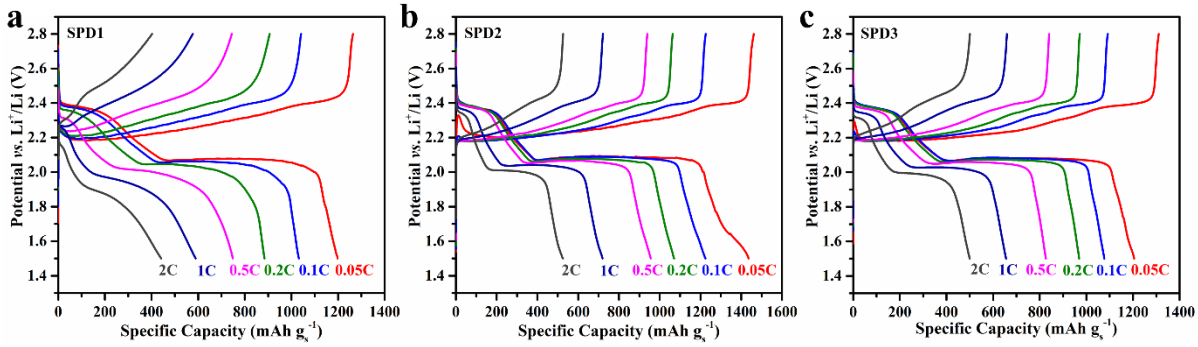

Figure S20. The discharge-charge curves under various C-rates of the cells based on (a) SPD1, (b) SPD2 and (c) SPD3.

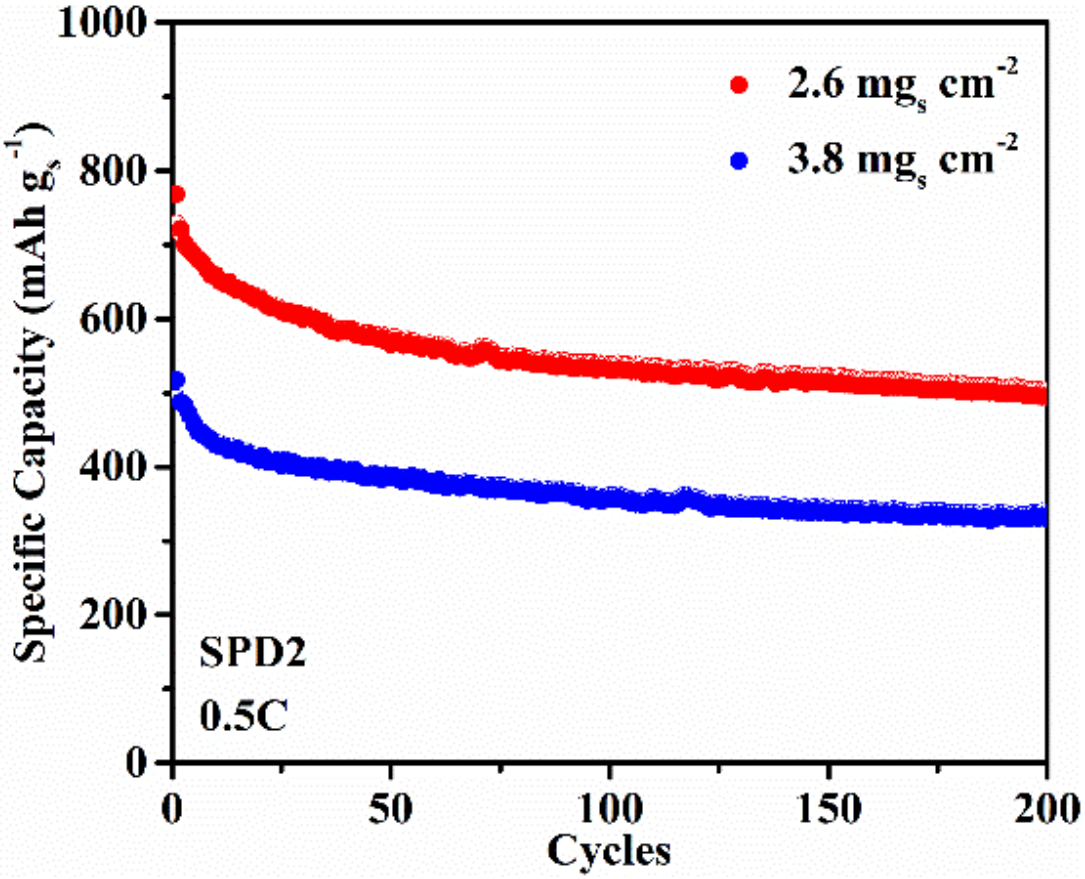

Figure S21. Long term cycling test for SPD2 under 0.5C with the sulfur loadings of 2.6 and 3.8 mg_s cm^{-2} (electrolyte: sulfur ratios of 15 and 10 µL mg_s^{-1}, respectively). The electrodes discussed in the manuscript had sulfur loadings of 1.4-1.6 mg cm^{-2} and were prepared using a doctor blade gap of 200 µm. Higher sulfur-loading electrodes were obtained by increasing the doctor blade gap to 300 and 400 µm, yielding sulfur loadings of 2.6 and 3.8 mg cm^{-2}.

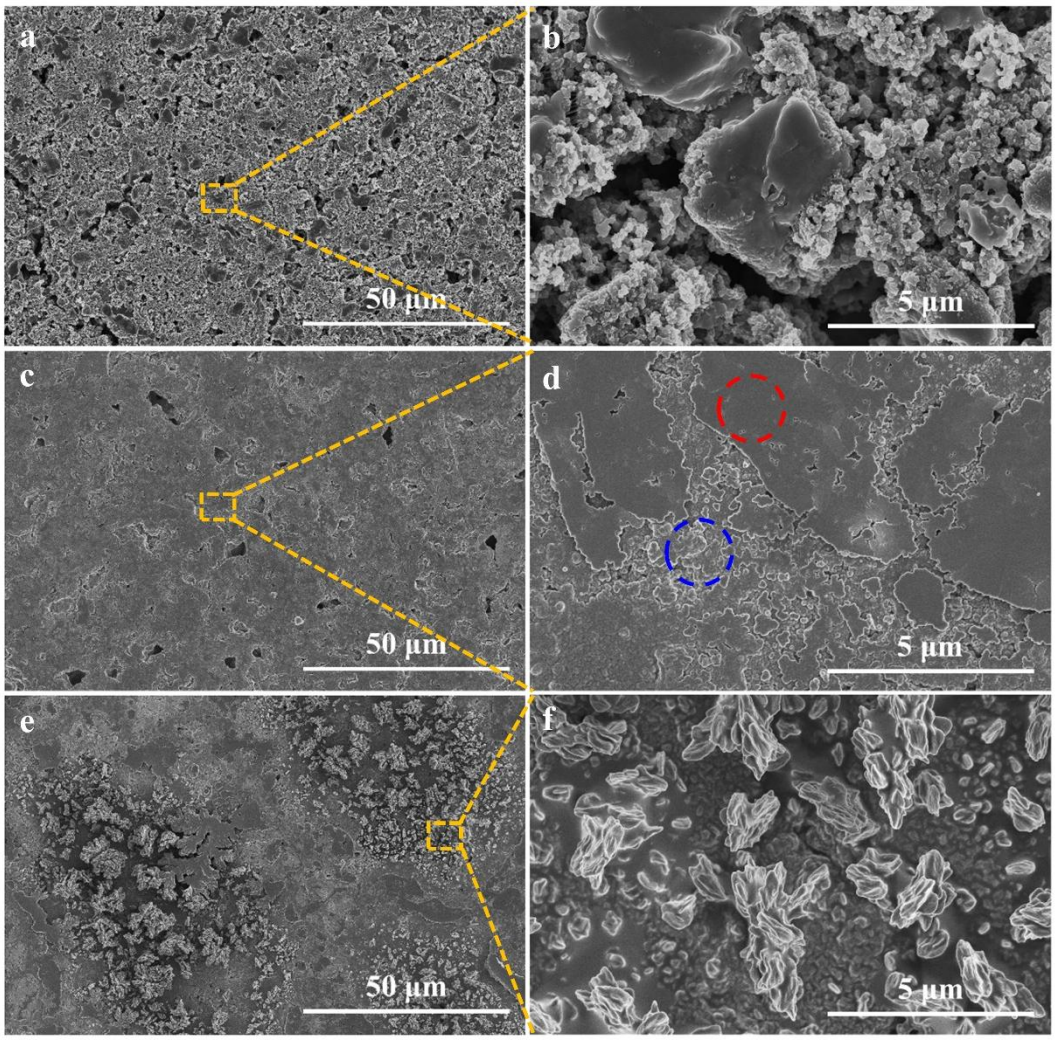

Figure S22. The SEM images of the initial electrodes based on SPD1 before the electrochemical characterisation: (a) Low magnification and (b) high magnification. The SEM images of electrodes based on SPD1 after 200 discharge-charge cycles: (c, e) Low magnification and (d, f) high magnification in two different areas.

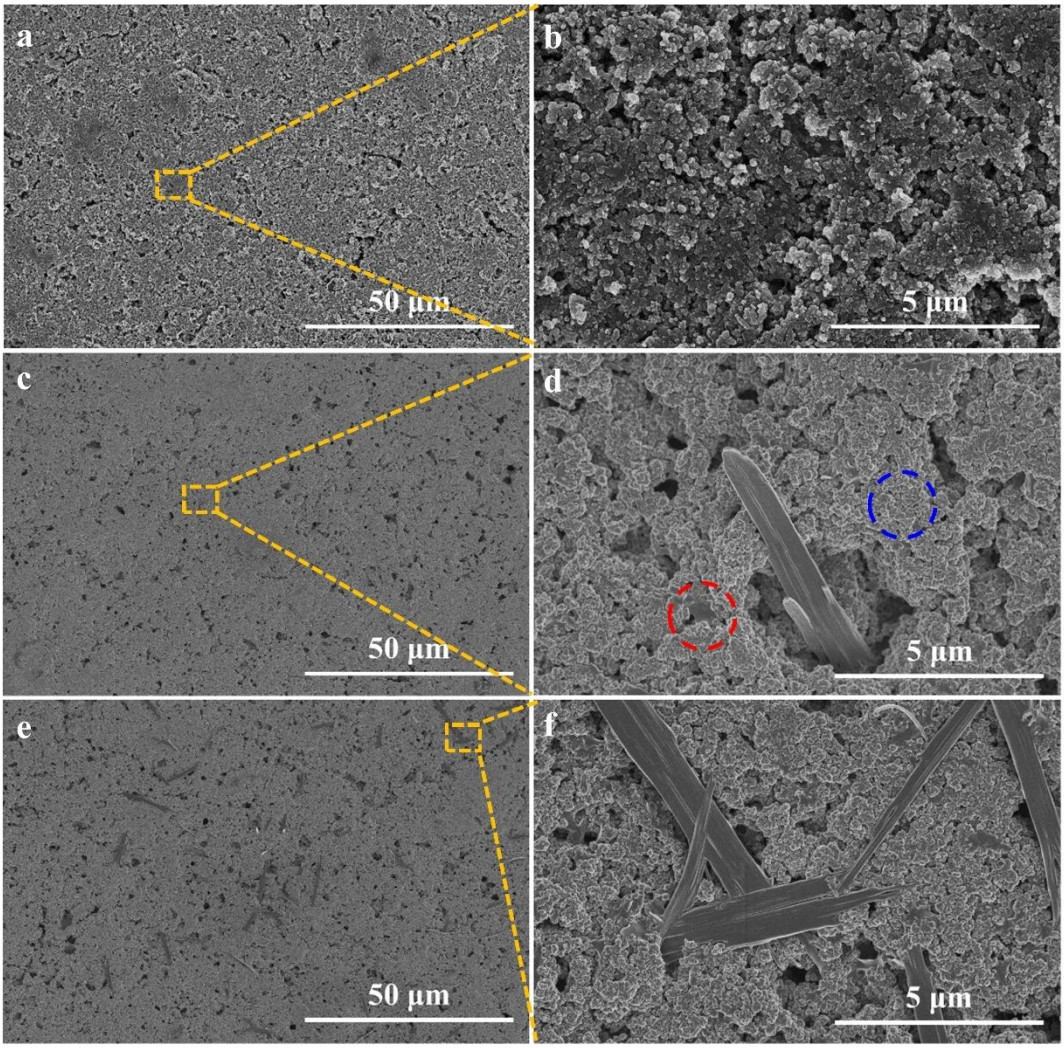

Figure S23. The SEM images of the initial electrodes based on SPD2 before the electrochemical characterisation: (a) Low magnification and (b) high magnification. The SEM images of electrodes based on SPD2 after 200 discharge-charge cycles: (c, e) Low magnification and (d, f) high magnification in two different areas.

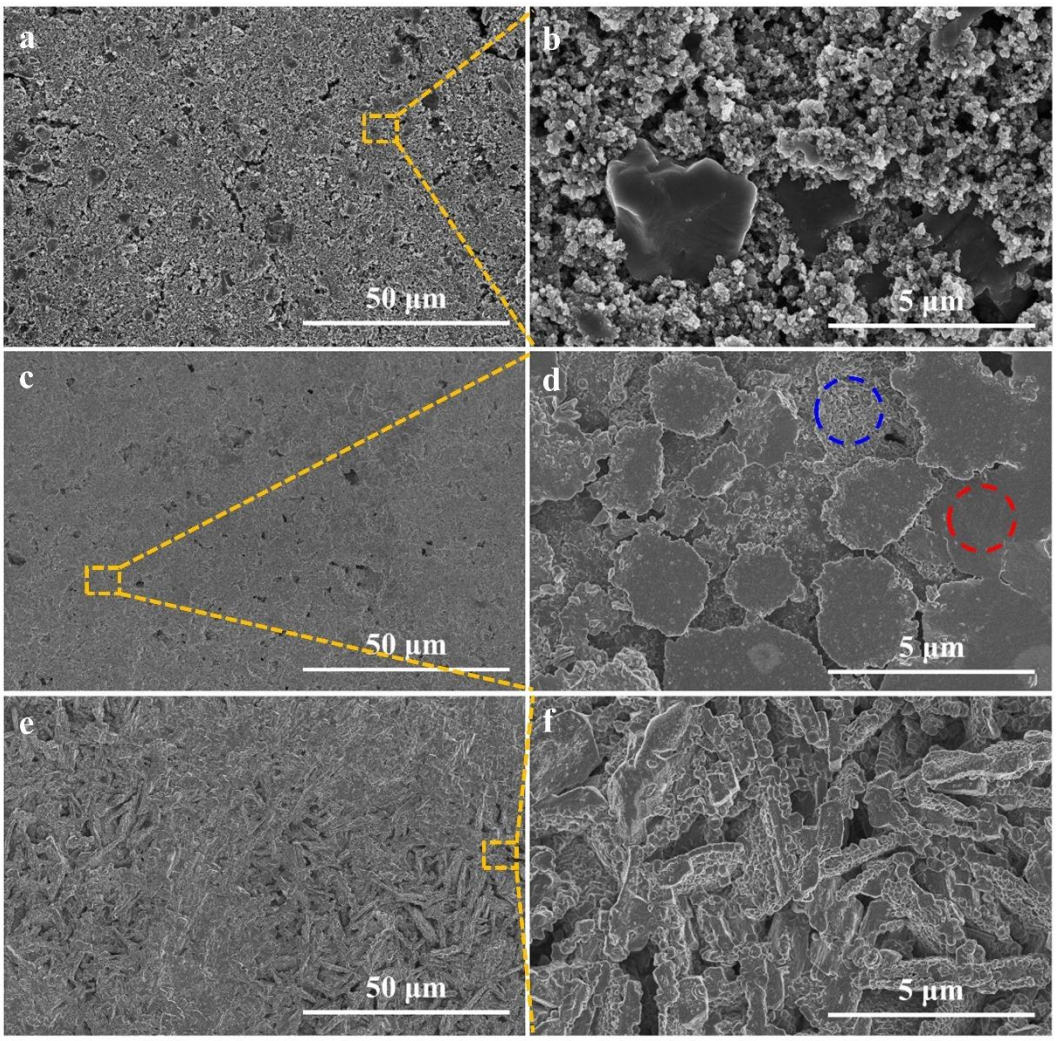

Figure S24. The SEM images of the initial electrodes based on SPD3 before the electrochemical characterisation: (a) Low magnification and (b) high magnification. The SEM images of electrodes based on SPD3 after 200 discharge-charge cycles: (c, e) Low magnification and (d, f) high magnification in two different areas.

Chemical confinement investigation

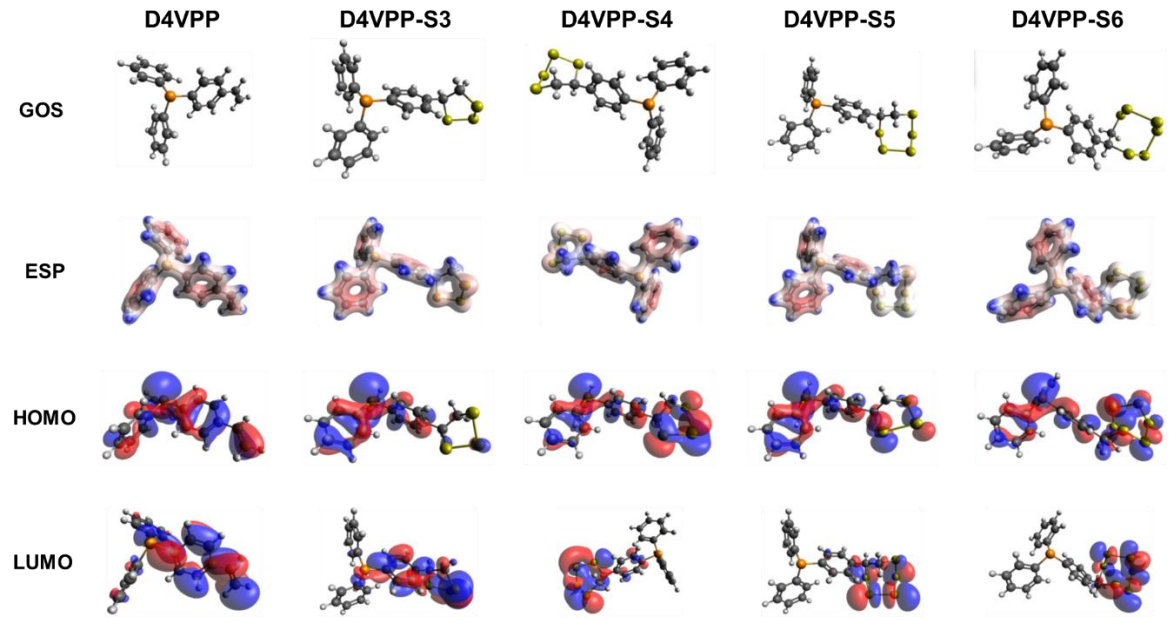

Figure S25. Geometry optimised structure, ESP maps and HOMO/LUMO energy levels of reacted and unreacted D4VPP monomers obtained by DFT calculations.

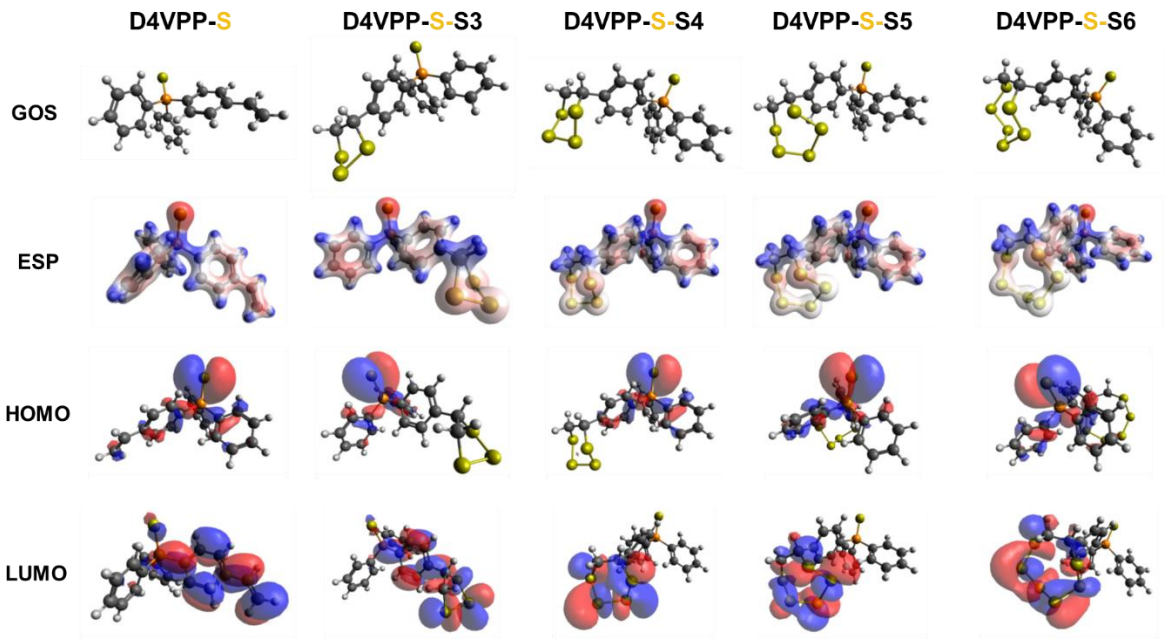

Figure S26. Geometry optimised structure, ESP maps and HOMO/LUMO energy levels of reacted and unreacted D4VPP-S monomers obtained by DFT calculations.

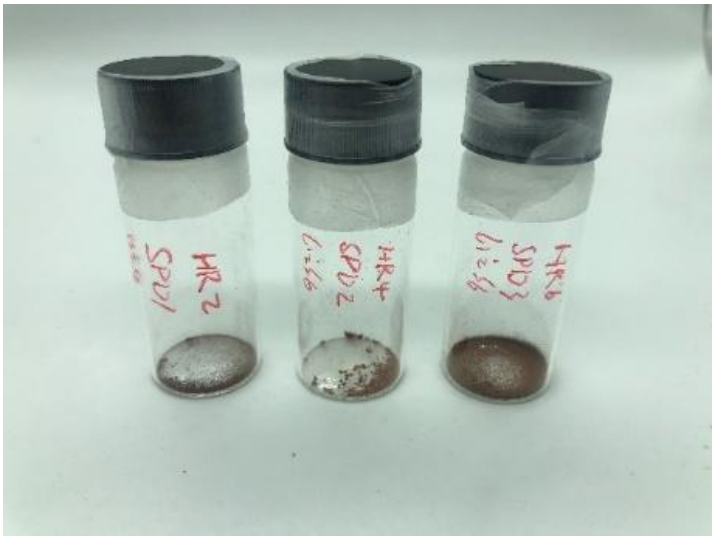

Figure S27. Photograph of SPD samples after immersion in Li_2S_6 solution.

Table S1. The BET results of SPD2 polymers.

Sample	BET surface area (m^2 g^{-1})
SPD1	-
SPD2	4.8
SPD3	-

Table S2. The results of SPD polymers in CHNS test

Polymers		**S (%)**	**C (%)**	**H (%)**	**other (%)**	**C/H**
SPD1	Calc.	80.00	17.42	1.50	1.08 (P)	11.62
	Anal.	80.00	16.87	1.80	1.33 (P+O)	9.37
SPD2	Anal.	81.50	13.59	1.41	3.77 (P+O)	11.92
SPD3	Anal.	76.50	20.07	1.88	1.55 (P+O)	10.68

Table S3. The HPLC results of elemental sulfur and SPD polymers.

Samples	Peak location (min)	Peak height	Area integration	Sulfur proportion* (%)
Toluene	6.843	49.8	483.1	/
S8	7.141	2542.6	44512.2	100
SPD1	6.976	501	5039.2	10.3
SPD2	7.003	504.7	5121.1	10.5
SPD3	6.995	292.2	2938.6	5.5

* The sulfur proportion was calculated via dividing the area integration values of polymers by area integration value of elemental sulfur after removing the influence of toluene.

Table S4. The active sulfur contents in the SPD polymers obtained by TGA analysis.

Polymers	SPD1	SPD2	SPD3
Active sulfur (%)	72.6	68.9	68.1

Table S5. Comparison of electrochemical performance between SPD samples with other inverse vulcanised cathode materials in recent publications.

Materials	Active sulfur content	Specific capacity (mAh g_s^{-1}) / current density of long-term test	Cycles / capacity decline % per cycle	reference
SPD1	72.6%	787 / 0.5C	500 / 0.055%	our work
SPD2	68.9%	976 / 0.5C	500 / 0.046%	our work
SPD3	68.1%	840 / 0.5C	500 / 0.051%	our work
Poly(sulfur-co-1-vinyl-3-allylimidazolium bromide)	63%	701 / 1C	150 / 0.060%	[3]
Polypyrrole-sulfur-covalent triazine framework	83%	703 / 0.5C	500 / 0.026%	[4]
Poly(tetrafluorohydroquinone)-sulfur	71%	905 / 0.5C	600 / 0.020%	[5]
S-poly(3-[(2-acryloyloxy) methyl]) thiophenes	74%	1080 / 0.2C	100 / 0.583%	[6]
Fibrous sulfurised trithiocyanuric acid@polyacrylonitrile	58%	896 / 1C	200 / 0.148%	[7]
Poly(sulfur-random-4-vinyl-1,2-epoxycyclohexane)	70%	800 / 0.5C	400 / 0.028%	[8]
Poly(Li_2S_6-r-1,3-10 wt% diisopropenylbenzene)	43%	1200 / 0.1 A g^{-1}	120 / 0.184%	[9]
Poly(S-r-squalene)	70%	401 / 0.1C	400 / 0.039%	[10]
Poly(4-(thiophene-3-yl) benzenethiol)	66.8%	756 / 0.2C	100 / 0.200%	[11]
Poly(vinyl trimethoxysilane-co-sulfur)	49.7%	850 / 0.5 A g^{-1}	500 / 0.095%	[12]
Sulfur-ethylene glycol dimethacrylate-dicyclopentadiene	73%	864 / 0.2C	200/0.093%	[13]

References

[1]. P. H. Maag, F. Feist, H. Frisch, P. W. Roesky and C. Barner-Kowollik, Macromolecules, 2022, 55, 9918-9924.

[2]. A. Kusumaatmaja, T. Ando, K. Terada, S. Hirohara, T. Nakashima, T. Kawai, T. Terashima and M. Tanihara, Journal of Polymer Science Part A: Polymer Chemistry, 2013, 51, 2527-2535.

[3]. X. Liu, Y. Lu, Q. Zeng, P. Chen, Z. Li, X. Wen, W. Wen, Z. Li and L. Zhang, ChemSusChem, 2020, 13, 715.

[4]. J. Kim, A. Elabd, S. Y. Chung, A. Coskun and J. W. Choi, Chemistry of Materials, 2020, 32, 4185.

[5]. W. Yan, K. Y. Yan, G. C. Kuang and Z. Jin, Chemical Engineering Journal, 2021, 424, 130316.

[6]. S. Yeşilot, S. Küçükköylü, T. Mutlu, E. Demir and R. Demir-Cakan, Mater Chem Phys 2022.

[7]. M. A. Weret, C.-F. J. Kuo, W.-N. Su, T. S. Zeleke, C.-J. Huang, N. A. Sahalie, T. A. Zegeye, Z. T. Wondimkun, F. W. Fenta, B. A. Jote, M.-C. Tsai and B. J. Hwang, Journal of Power Sources, 2022, 541, 231693.

[8]. T. Zhang, F. Hu, W. Shao, S. Liu, H. Peng, Z. Song, C. Song, N. Li and X. Jian, ACS nano, 2021, 15, 15027-15038.

[9]. F. Dong, C. Peng, H. Xu, Y. Zheng, H. Yao, J. Yang and S. Zheng, ACS nano, 2021, 15, 20287-20299.

[10]. L. Djuandhi, N. Sharma, B. C. Cowie, T. V. Nguyen and A. Rawal, Physical Chemistry Chemical Physics, 2021, 23, 14075-14092.

[11]. J. Ning, H. Yu, S. Mei, Y. Schütze, S. Risse, N. Kardjilov, A. Hilger, I. Manke, A. Bande and V. G. Ruiz, ChemSusChem, 2022, 15, e202200434.

[12]. L. Zhao, F. Qiu, X. Deng, Y. Huang, Y. Li, C. Zhao, W. Ren, C. Zou, X. Li and M. Wang, ACS Applied Energy Materials, 2022, 5, 7617-7626.

[13]. H. Wang, B. Zhang, R. Dop, P. Yan, A. R. Neale, L. J. Hardwick and T. Hasell, Journal of Power Sources, 2022, 545, 231921.